Vibroacoustic Behaviour of a Fluid-Filled Baffled Cylindrical Shell Submerged in a Shallow-Water Waveguide

Jamie Kha, Mahmoud Karimi, Laurent Maxit

Acoustics Australia
https://doi.org/10.1007/s40857-025-00358-y

ORIGINAL PAPER

Vibroacoustic Behaviour of a Fluid-Filled Baffled Cylindrical Shell Submerged in a Shallow-Water Waveguide

Jamie Kha[1] · **Mahmoud Karimi**[1] · **Laurent Maxit**[2]

Received: 7 April 2025 / Accepted: 3 August 2025

Abstract
An analytical method for predicting the forced vibroacoustic response of a fluid-filled baffled cylindrical shell submerged in a shallow-water waveguide is presented. The structural equations are governed by a thin shell theory that is decomposed into circumferential modes with a Fourier series and axial modes using a beam function. Heavy fluid fills the exterior and interior domains of the shell. The exterior fluid domain is further constrained by acoustic boundaries of an upper free surface and lower rigid bottom, which together form an ideal shallow-water waveguide. The acoustic boundaries are enforced by employing the image source method and Graf's addition theorem which reconciles the differing coordinate systems of the many image sources that appear in the analytical expressions for the fluid–structure coupling. Vibroacoustic characteristics due to a mechanical point excitation on the surface of the shell or acoustic excitation from an internal monopole source and influence of different waveguide depths are investigated.

Keywords Fluid-filled finite baffled cylindrical shell · Shallow-water waveguide · Underwater vibroacoustics · Image source method · Analytical model · Mechanical point excitation · Acoustic monopole source excitation

1 Introduction

Vibroacoustic analysis of cylindrical structures is of interest as it can provide a relevant model for engineering applications such as underwater acoustics and geotechnical applications; for instance, fluid-filled cylindrical shells can represent pipelines, ballast tanks of ships, and underwater vehicles. The analysis of shells [1–3] and its underwater acoustics [4] can be found in literature as a basis for the analytical investigation of underwater cylindrical shells. Typically, cylindrical shells are studied in an acoustic free field (i.e. infinite sea) [5–11] such as in investigations related to acoustic scattering characteristics of shells [7, 8], and predicting flow-induced noise in pipes [9–11]. The presence of acoustic boundaries such as a sea surface or sea floor in the analysis can be relevant for different underwater operating conditions such as the effect of a sea surface on partially submerged shells [12–16] and completely submerged shells near an acoustic boundary such as a free surface [17–20]. A general approach to tackle such vibroacoustic models is to build them with element-based models such as the finite element method (FEM), boundary element method (BEM), or coupled FEM-BEM approaches [21–23]. This numerical framework can be computationally expensive, especially as the spatial resolution of analysis increases with increasing frequencies in the frequency-domain analyses or large fluid domains, especially when evaluating the far-field acoustic propagation. It is asserted that analytical (and semi-analytical) approaches provide an avenue to make such predictions more manageable. However, analytical approaches rely on simplicity such that models can be amenable for analysis, and specifically for cylindrical structures are reduced to thin infinitely long shells. In literature, the vibroacoustic behaviour of cylindrical shells is exhibited via mechanical line excitations [19, 20, 24, 25], which reduce the system of an infinitely long thin shell to being a mechanical point-excited thin annulus (i.e. a two-dimensional study). To consider a three-dimensional study, a mechanical point-excited infinitely long thin shell is presented in a fluid domain that is terminated by an upper free surface [19] and recently in an ideal shallow-water waveguide [26]. Shells of finite

✉ Jamie Kha
jamie.kha@uts.edu.au

[1] Centre for Audio, Acoustics and Vibration, University of Technology Sydney, Sydney, NSW, Australia

[2] Laboratoire Vibrations-Acoustique (LVA), INSA–Lyon, Villeurbanne Cedex 69621, France

Published online: 16 October 2025

length can be analytically investigated with infinitely rigid baffles attached at its ends, such that specific axial boundary conditions are enforced at the interface between the elastic shell and rigid baffle [3, 16, 27, 28]. However, these studies have been limited to simple fluid domains such as an acoustic free field [3, 27] or in an acoustic half-space [28].

Theoretical forced vibroacoustic analysis of fluid-loaded cylindrical shells has been typically conducted within an acoustic free field as to ignore the influence of surrounding acoustic boundaries that could be present in an ocean environment. Recent studies have focused on complicating other aspects of the vibroacoustics system such as imposing stochastic excitation rather than a deterministic excitation. Maxit et al. [9] presented an analytical model formulation of an infinitely long shell that is excited by a turbulent boundary layer, while, for finite-length baffled shells, the analysis has been presented in pre-stressed fluid-loaded cylindrical shells by Guo et al. [27], which can be recognised as a study that builds upon predecessors such as Sandman [29], Laulagnet and Guyader [30], and Junger and Feit [3]. It is also mentioned that theoretical analysis can be performed with hybrid approaches that combine analytical solutions with numerical methods to tackle complex geometries in which analytical models can no longer solve. For example, the condensation transfer function approach [25, 31, 32], seen as a modular sub-structuring framework to decompose a target vibroacoustic system and re-compile a predicted behaviour, can benefit from employing theoretical solutions where possible. These works can serve as a motivation to pursue advancements in the analytical models involving the vibroacoustic behaviour of cylindrical shells.

The addition of acoustic boundaries enforces a different fluid–structure coupling, and the external fluid domain can no longer be considered an infinite sea (acoustic free field). A sequence of theoretical developments can be observed in the literature, from first involving a single boundary, typically of a pressure release boundary condition of a free surface [15, 19, 20]. In Li et al. [19], far-field acoustic responses of a point-excited infinitely long cylindrical shell are analytically predicted, while, in Marsick et al. [20], the simpler two-dimensional problem is solved by considering a line-distributed load of an infinitely long shell. Near and far-field characteristics were investigated for a fluid-filled two-dimensional cylindrical shell. In contrast, Guo et al. [15] developed a framework that couples the analytical solution for the vibration of a shell with the acoustic propagation prediction from the BEM to predict far-field acoustic pressure from a finite-length cylindrical shell. Then, there are examples of double reflection scenarios, which can be viewed as an extension to the acoustic half-space (semi-infinite fluid domain). In this case, a horizontal free surface meets an adjacent vertical rigid floor to form a quarter-infinite fluid domain. It was analysed as a two-dimensional problem by Chen et al. [33] and Guo et al [34]. These investigations progress the complexity of the fluid domain in which the cylindrical shells are coupled to. A relevant advancement would be involving a shallow-water environment, where two parallel acoustic boundaries form an acoustic shallow-water waveguide. The free vibration analysis has been performed by Wang et al. [35]; however, they neglected the fluid–structure coupling of the shallow-water waveguide. This approach is known as the "mirror effect" model and has been demonstrated in the literature [20, 24] to be incomplete in modelling the waveguide reflection phenomenon. In general, a combined FEM-BEM solver such as suggested in Jiang et al. [23] and Zhang et al. [36] can be applied. This is similar to the previously mentioned study of Guo et al. [15]; however, with a coupled FEM-BEM solver, the analytical solution for vibration is replaced with FEM. Most works related to a shallow-water waveguide can be found in the field of underwater acoustics, with applications to oceanography. However, structural vibration is typically not involved, for example, in the study of acoustic scattering of rigid and fluid cylinders by Baynes et al. [37] which focuses on acoustic propagation. A typical approach to model the shallow-water waveguide is with the image source method. In terms of vibroacoustics, it suggests the acoustic component that is modelled analytically by the image source method can be coupled with the vibration component of a cylindrical shell that can also be solved analytically. This analytical approach is presented in Kha et al. [24] for a two-dimensional setting and Kha et al. [26] for a three-dimensional setting involving an infinitely long shell under point load. However, the investigation for the case of a finite-length cylindrical shell remains open.

This paper herein provides an analytical framework for predicting the forced vibroacoustic responses of a fluid-filled finite-length baffled cylindrical shell submerged in an ideal shallow-water waveguide. Its structural dynamics are described by a thin shell theory, while the acoustics of the internal and external fluid domains are governed by the Helmholtz equation. More specifically, the acoustic boundaries of the external fluid domain of an ideal shallow-water waveguide are enforced by applying the image source method. Under this approach, the acoustic reflections off the upper free surface and lower rigid bottom are represented by many image sources. Graf's addition theorem is employed to reconcile the differing coordinate systems of the many image sources that appear in the analytical expressions for the external fluid loading. It is also at this stage in the model that the structural dynamics become coupled with the acoustics of the shallow-water waveguide by considering the continuity between the shell radial velocity and fluid radial velocity at the interface between the structure and external fluid domain. It is referred to as fluid–structure coupling. The vibroacoustic behaviour is exhibited due to a mechanical point excitation

or acoustic excitation from an internal monopole source. The acoustic excitation is the blocked pressure at the internal surface of the shell due to the internal monopole source. The analytical framework is applied to a specific numerical example and compared against an equivalent model using the finite element method (FEM) via the COMSOL Multiphysics v6.1 software. Both structural and acoustic characteristics from the numerical example are compared to verify the proposed method. Finally, the excited shell submerged in different waveguide fluid domains is investigated. Convergence of its vibroacoustic behaviour to simpler fluid domains of an acoustic free field (infinite sea) and acoustic half-spaces with an upper free surface only or a lower rigid floor only are demonstrated as the waveguide depths increase. The influence of the waveguide is mainly observed in the low frequency portion of the radiated sound power.

2 Analytical Framework

The system of interest consists of a finite cylindrical thin shell baffled on each end by infinitely long rigid cylinders. Both the exterior and interior of the cylindrical shell are occupied by a fluid. The external fluid domain is further restricted by acoustic boundaries of an upper free surface and lower rigid bottom, which together form the fluid domain of an ideal shallow-water waveguide. The geometry of the shell is specified by a uniform thickness h, mean radius R, an inner radius $R_{\text{int}} = R - h/2$, outer radius $R_{\text{ext}} = R + h/2$, and half-length L (i.e. a total length of $2L$). Subsequent analysis is in the frequency domain (omitting the time dependence of $\mathrm{e}^{-\mathrm{j}\omega t}$) such that the shell material properties include a complex Young's modulus $E = \bar{E}\left(1 - \eta_s \mathrm{j}\right)$ ($\bar{E}$ being the typical Young's modulus) where η_s is a structural loss damping factor and $\mathrm{j} = \sqrt{-1}$, Poisson's ratio μ, and shell density ρ_s. While the external and internal fluid domains are filled with fluids of densities ρ_f^{ext} and ρ_f^{int}, respectively, and characterised by complex sound speeds c^{ext} and c^{int}, respectively, where $c = \bar{c}\left(1 - \eta_f \mathrm{j}\right)$ ($\bar{c}$ being the typical sound speed) with fluid damping η_f. A schematic of the system of interest is shown in Figure 1, both in Cartesian coordinates (x, y, z) and cylindrical coordinates (r, φ, z), where the origin is positioned at the centre of the shell. The external fluid domain of an ideal shallow-water waveguide has a total depth $H = H_{fs} + H_{sb}$, where the distance between the centre of the shell and upper free surface is H_{fs} and lower rigid bottom (seabed) is H_{sb}. Both the external and internal fluid domains are of infinite extent along the z-axis.

2.1 Structural Dynamics

The motions of the cylindrical shell are represented by the governing equations of a thin shell theory [1]

$$[\mathbf{L}]\begin{bmatrix} u \\ v \\ w \end{bmatrix} = \gamma \begin{bmatrix} 0 \\ 0 \\ f_e - f_l^{\text{ext}} + f_l^{\text{int}} \end{bmatrix}, \tag{1}$$

where $[\mathbf{L}]$ is the Flügge's operator, $\gamma = R^2\left(1 - \mu^2\right)/E^* h$, f_e, f_l^{ext}, f_l^{int} are the pressure distributions due to the external source, the external fluid loading and the internal fluid loading, respectively. The axial, tangential and radial displacements, u, v, w, respectively, are decomposed circumferentially as a Fourier series in n, and axially with a beam function in m, thus taking the following form [1, 3]

$$\begin{aligned} \begin{pmatrix} u(\varphi, z) \\ v(\varphi, z) \\ w(\varphi, z) \end{pmatrix} &= \sum_{n=-\infty}^{\infty} \mathrm{e}^{\mathrm{j}n\varphi} \begin{pmatrix} U_n(z) \\ V_n(z) \\ W_n(z) \end{pmatrix} \\ &= \sum_{n=-\infty}^{\infty} \mathrm{e}^{\mathrm{j}n\varphi} \sum_{m=0}^{\infty} \begin{pmatrix} \tilde{U}_{mn} X'_m(z) \\ \tilde{V}_{mn} X_m(z) \\ \tilde{W}_{mn} X_m(z) \end{pmatrix}, \end{aligned} \tag{2}$$

where $\tilde{U}_{mn}$, $\tilde{V}_{mn}$ and $\tilde{W}_{mn}$ are the Fourier coefficients of axial, tangential and radial displacements, respectively, $X_m(z)$ is the appropriate beam functions of axial mode m (and $X'_m(z)$ its derivative with respect to the argument) that satisfy the boundary conditions enforced at the connections with the rigid baffles. Moreover, the external pressure distributions are decomposed in a similar manner to the radial displacement

$$\begin{aligned} \begin{pmatrix} f_e(\varphi, z) \\ f_l^{\text{ext}}(\varphi, z) \\ f_l^{\text{int}}(\varphi, z) \end{pmatrix} &= \sum_{n=-\infty}^{\infty} \mathrm{e}^{\mathrm{j}n\varphi} \begin{pmatrix} F_{e,n}(z) \\ F_{l,n}^{\text{ext}}(z) \\ F_{l,n}^{\text{int}}(z) \end{pmatrix} \\ &= \sum_{n=-\infty}^{\infty} \mathrm{e}^{\mathrm{j}n\varphi} \sum_{m=0}^{\infty} \begin{pmatrix} \tilde{F}_{e,mn} X_m(z) \\ \tilde{F}_{l,mn}^{\text{ext}} X_m(z) \\ \tilde{F}_{l,mn}^{\text{int}} X_m(z) \end{pmatrix}, \end{aligned} \tag{3}$$

$$\begin{aligned} \begin{pmatrix} \tilde{F}_{e,mn} \\ \tilde{F}_{l,mn}^{\text{ext}} \\ \tilde{F}_{l,mn}^{\text{int}} \end{pmatrix} &= \frac{1}{L}\int_{-L}^{L} \frac{1}{2\pi}\int_{0}^{2\pi} \\ &\qquad \begin{pmatrix} f_e(\varphi, z) \\ f_l^{\text{ext}}(\varphi, z) \\ f_l^{\text{int}}(\varphi, z) \end{pmatrix} \mathrm{e}^{-\mathrm{j}n\varphi} X_m^*(z)\, d\varphi\, dz, \end{aligned} \tag{4}$$

for $z \in [-L, L]$ and $\varphi \in [0, 2\pi)$, where * refers to the complex conjugate, and, $\tilde{F}_{e,mn}$, $\tilde{F}_{l,mn}^{\text{ext}}$ and $\tilde{F}_{l,mn}^{\text{int}}$ are the Fourier coefficients of the pressure distributions due to the external source, the external fluid loading and the internal fluid loading, respectively. In the following developments, a shell with simply supported ends (i.e. such that the displacements in the x- and y-direction are constrained to be zero, while the displacement in the z-direction is free) is considered. Therefore, the beam functions are $X_m(z) = \cos(k_m z)$ for $|z| \leq L$ and 0 otherwise, $k_m = (m + 1/2)\pi/L$, and $X'_m(z) = -\sin(k_m z)$

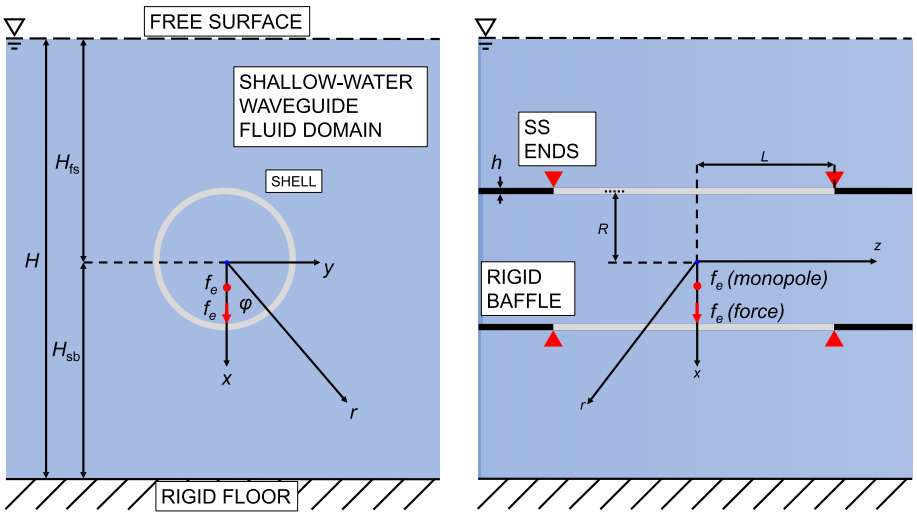

Fig. 1 Schematic of a fluid-filled finite-length simply supported (SS) baffled shell in a shallow-water waveguide

for $|z| \leq 0$ and 0 otherwise [1]. After considering the appropriate orthogonality relations, the modal governing equations that are represented in m, n are

$$\left[\tilde{\mathbf{L}}\right]\begin{bmatrix}\tilde{U}_{mn}\\ \tilde{V}_{mn}\\ \tilde{W}_{mn}\end{bmatrix} = \gamma\begin{bmatrix}0\\ 0\\ \tilde{F}_{e,mn} - \tilde{F}^{\text{ext}}_{l,mn} + \tilde{F}^{\text{int}}_{l,mn}\end{bmatrix}, \tag{5}$$

where the elements of $\left[\tilde{\mathbf{L}}\right]$ can be found in Ref. [19, 26]. The coefficients for the radial displacements $\tilde{W}_{mn}$ are solved for by applying Cramer's rule

$$\frac{\left|\tilde{\mathbf{L}}\right|}{\tilde{\mathbf{L}}_{11}\tilde{\mathbf{L}}_{22} - \tilde{\mathbf{L}}_{12}\tilde{\mathbf{L}}_{21}}\tilde{W}_{mn} = \gamma\left(\tilde{F}_{e,mn} - \tilde{F}^{\text{ext}}_{l,mn} + \tilde{F}^{\text{int}}_{l,mn}\right). \tag{6}$$

The radial excitation forcing term f_e is specified as an input, while the external and internal fluid loading terms, f_l^{ext} and f_l^{int}, respectively, are determined by considering the motions of each fluid domain and applying the continuity relations at the appropriate fluid–structure interfaces.

2.2 External Fluid Loading

2.2.1 Acoustic Propagation into the External Fluid

In an acoustic free field, the external acoustic pressure $p^{\text{ext, FF}}$ obeys the Helmholtz equation under the Sommerfeld radiation condition. In cylindrical coordinates, and using a method of separation of variables, the solution is known to take the general form [2]

$$p^{\text{ext, FF}}(r, \varphi, z) = \frac{1}{2\pi}\sum_{n=-\infty}^{\infty} \mathrm{e}^{\mathrm{j}n\varphi}\int_{-\infty}^{\infty} \tilde{P}_n^{\text{ext}}(k_z)\, H_n^{(1)}\left(k_r^{\text{ext}} r\right)\mathrm{e}^{\mathrm{j}k_z z}\, dk_z, \tag{7}$$

where $H_n^{(1)}(\,)$ is the Hankel function of the first kind, k_z is the axial wavenumber, $k^{\text{ext}} = \omega/c^{\text{ext}}$ is the complex acoustic wavenumber in the exterior fluid domain, and $k_r^{\text{ext}} = \sqrt{k^{\text{ext}2} - k_z^2}$ is the associated radial wavenumber. In a shallow-water waveguide, the external acoustic propagation will interact with the upper free surface and lower rigid bottom.

The total acoustic pressure p^{ext} is taken to be the sum of successive acoustic pressures

$$p^{\text{ext}}(r, \varphi, z) = \frac{1}{2\pi}\sum_{i=-\infty}^{\infty}\left\{\sum_{n=-\infty}^{\infty}\mathrm{e}^{\mathrm{j}n\varphi^i}\int_{-\infty}^{\infty}\tilde{P}_n^{\text{ext},i}(k_z)\, H_n^{(1)}\left(k_r^{\text{ext}} r^i\right)\mathrm{e}^{\mathrm{j}k_z z^i}\, dk_z\right\}, \tag{8}$$

where the original or "real" source is indexed as $i = 0$ $(r^0, \varphi^0, z^0 = r, \varphi, z)$ and "image" sources are indexed as $i \neq 0$ and represent the reflections off the acoustic boundaries of the shallow-water waveguide fluid domain. Image sources that instantiate with a reflection off the lower rigid bottom are considered lower image sources (i.e. $i < 0$), and those off the upper free surface are considered upper image sources (i.e. $i > 0$). The coordinates of the image sources are related to the original coordinate system by the following relations [20, 26]

$$r^i = \begin{cases}\sqrt{\left[D^i - r\cos(\varphi)\right]^2 + \left[r\sin(\varphi)\right]^2} & i < 0,\\ \sqrt{\left[D^i + r\cos(\varphi)\right]^2 + \left[r\sin(\varphi)\right]^2} & i \geq 0,\end{cases} \tag{9}$$

$$\varphi^i = \begin{cases}\pi - \arctan\left[\dfrac{r\sin(\pi - \varphi)}{D^i + r\cos(\pi - \varphi)}\right] & i < 0,\\ \arctan\left[\dfrac{r\sin(\varphi)}{D^i + r\cos(\varphi)}\right] & i \geq 0,\end{cases} \tag{10}$$

where D^i is the distance between the origin of the i-th image source coordinate system to the original coordinate system, and $z^i = z$.

2.2.2 External Fluid-Shell Coupling

A continuity relation is enforced at the interfaces between the outer surface of the shell and external fluid domain, which captures the fluid-shell coupling. The shell is an elastic region that spans between $|z| \leq L$ (i.e. a total length of $2L$) and is held by infinitely long rigid baffles that spans $|z| > L$. The continuities between the shell radial velocity and fluid velocity at the respective fluid domains are

$$\left.\frac{\partial p^{\text{ext}}}{\partial r}\right|_{r=R_{\text{ext}}} = \begin{cases} -\omega^2 \rho_f^{\text{ext}} w, & |z| \leq L, \\ 0, & |z| > L. \end{cases} \tag{11}$$

The radial displacement from Eq. (2) and external acoustic pressures from Eq. (8) is substituted into Eq. (11) to obtain the following expression

$$\begin{aligned} &\frac{\partial}{\partial r}\left\{\frac{1}{2\pi}\sum_{i=-\infty}^{\infty}\sum_{n=-\infty}^{\infty} \mathrm{e}^{\mathrm{j}n\varphi^i}\int_{-\infty}^{\infty}\tilde{P}_n^{\text{ext},i}\left(k_z\right)\right. \\ &\left.H_n^{(1)}\left(k_r^{\text{ext}} r^i\right)\mathrm{e}^{\mathrm{j}k_z z^i}\,dk_z\right\}\Big|_{r=R_{\text{ext}}} \\ &= \omega^2\rho_f^{\text{ext}}\sum_{n=-\infty}^{\infty}\mathrm{e}^{\mathrm{j}n\varphi}\sum_{m=0}^{\infty}\tilde{W}_{mn}X_m\left(z\right). \end{aligned} \tag{12}$$

Total acoustic pressure in the external fluid domain contains image sources, each with its own coordinate system with origins positioned at its centre. To reconcile the different coordinate systems, the Graf's addition theorem is applied to convert the Hankel function and complex exponential functions into terms in the coordinate system of the real source (i.e. $r^i\big|_{r=R_{\text{ext}}}, \varphi^i, z^i \rightarrow R_{\text{ext}}, \varphi, z$). Consider the term inside the partial derivative of Eq. (12) evaluated at the outer surface of the shell

$$\begin{aligned} &\frac{1}{2\pi}\sum_{i=-\infty}^{\infty}\sum_{n=-\infty}^{\infty}\mathrm{e}^{\mathrm{j}n\varphi^i}\int_{-\infty}^{\infty}\tilde{P}_n^{\text{ext},i}\left(k_z\right) \\ &H_n^{(1)}\left(k_r^{\text{ext}} r^i\big|_{r=R_{\text{ext}}}\right)\mathrm{e}^{\mathrm{j}k_z z^i}\,dk_z \\ &= \frac{1}{2\pi}\sum_{n=-\infty}^{\infty}\mathrm{e}^{\mathrm{j}n\varphi}\int_{-\infty}^{\infty}\sum_{n''=-\infty}^{\infty}\Lambda_{nn''}\left(R_{\text{ext}}\right) \\ &\tilde{P}_{n''}^{\text{ext}}\left(k_z\right)\mathrm{e}^{\mathrm{j}k_z z}\,dk_z, \end{aligned} \tag{13}$$

where

$$\begin{aligned} \Lambda_{nn''}\left(R_{\text{ext}}\right)\tilde{P}_n^{\text{ext}}\left(k_z\right) &= \delta_{nn''}H_n^{(1)}\left(k_r^{\text{ext}}R_{\text{ext}}\right)\tilde{P}_{n''}^{\text{ext}}\left(k_z\right) + \\ &\sum_{i>0}(-1)^{n+n''}\,\tilde{P}_{-n''}^{\text{ext},i}\left(k_z\right)H_{n+n''}^{(1)}\left(k_r^{\text{ext}}D^i\right)J_n\left(k_r^{\text{ext}}R_{\text{ext}}\right) + \\ &\sum_{i<0}\tilde{P}_{-n''}^{\text{ext},i}\left(k_z\right)H_{n+n''}^{(1)}\left(k_r^{\text{ext}}D^i\right)J_n\left(k_r^{\text{ext}}R_{\text{ext}}\right), \end{aligned} \tag{14}$$

is from applying Graf's addition theorem

$$\begin{aligned} &H_{-n}^{(1)}\left(k_r^{\text{ext}}r^i\big|_{r=R_{\text{ext}}}\right)\mathrm{e}^{-\mathrm{j}n\varphi^i} = \\ &\begin{cases} \sum_{n''=-\infty}^{\infty}(-1)^{n+n''}\,H_{n+n''}^{(1)}\left(k_r^{\text{ext}}D^i\right)J_{n''}\left(k_r^{\text{ext}}r\right)\mathrm{e}^{\mathrm{j}n''\varphi}, & i>0 \\ \sum_{n''=-\infty}^{\infty}H_{n+n''}^{(1)}\left(k_r^{\text{ext}}D^i\right)J_{n''}\left(k_r^{\text{ext}}r\right)\mathrm{e}^{\mathrm{j}n''\varphi}, & i<0 \end{cases} \end{aligned} \tag{15}$$

to Eq. (13) for $r < D^i$ (which is the case considered for the acoustic pressure for external fluid-loading, i.e. $r = R_{\text{ext}}$), where D^i is the distance between the origin of the i-th image source coordinate system to the original coordinate system, and subsequently exchanging n and n'' without loss of generality. The spectral pressures of the image sources are related to the spectral pressures of the real source in an ideal shallow-water waveguide by [24, 26]

$$P_{-n''}^{\text{ext,i}} = \begin{cases} -P_{n''}^{\text{ext}}, -P_{-n''}^{\text{ext}}, +P_{n''}^{\text{ext}}, +P_{-n''}^{\text{ext}}, \ldots \text{ for } i>0, \\ +P_{n''}^{\text{ext}}, -P_{-n''}^{\text{ext}}, -P_{n''}^{\text{ext}}, +P_{-n''}^{\text{ext}}, \ldots \text{ for } i<0, \end{cases} \tag{16}$$

and

$$\delta_{nn''} = \begin{cases} 0 & \text{if } n \neq n'', \\ 1 & \text{if } n = n'', \end{cases}$$

is the Kronecker delta function. It is important to recognise in the relation from Eq. (16) that while the sign of the coefficients is repeating every four iterations, the sign of the circumferential mode orders is changing every two iterations. The change in sign of the circumferential mode orders (i.e. n'' to $-n''$ and vice versa) implies a complete mode reversal after every reflection off the acoustic boundary. The external fluid loading f_l^{ext} is equivalent to the acoustic pressure at the outer surface of the shell $p(r = R_{\text{ext}})$. Therefore, we substitute Eq. (13) into Eq. (8), evaluated at $r = R_{\text{ext}}$ and arrive at the following expression for fluid loading

$$\begin{aligned} f_l^{\text{ext}}\left(\varphi, z\right) &= p^{\text{ext}}\left(r = R_{\text{ext}}, \varphi, z\right) \\ &= \frac{1}{2\pi}\sum_{n=-\infty}^{\infty}\mathrm{e}^{\mathrm{j}n\varphi}\int_{-\infty}^{\infty}\sum_{n'=-\infty}^{\infty}\Lambda_{nn'}\left(R_{\text{ext}}\right)\tilde{P}_{n'}^{\text{ext}}\left(k_z\right)\mathrm{e}^{\mathrm{j}k_z z}\,dk_z. \end{aligned} \tag{17}$$

Now, to determine the spectral external pressures, Eq. (13) is introduced into Eq. (12) to obtain the following expression

$$\frac{k_r^{\text{ext}}}{2\pi}\sum_{n=-\infty}^{\infty} \mathrm{e}^{\mathrm{j}n\varphi}\int_{-\infty}^{\infty}\sum_{n''=-\infty}^{\infty}\Lambda'_{nn''}\left(R_{\text{ext}}\right)\tilde{P}_{n''}^{\text{ext}}\left(k_z\right)\mathrm{e}^{\mathrm{j}k_z z}\,dk_z = \omega^2\rho_f^{\text{ext}}\sum_{n=-\infty}^{\infty}\mathrm{e}^{\mathrm{j}n\varphi}\sum_{m=0}^{\infty}\tilde{W}_{mn}X_m\left(z\right), \tag{18}$$

where

$$\begin{aligned}\Lambda'_{nn''}\left(R_{\text{ext}}\right) &= \delta_{nn''}H_n'^{(1)}\left(k_r^{\text{ext}}R_{\text{ext}}\right)\\ &+\sum_{i>0}\alpha_{n''}^{i}\left(-1\right)^{n+n''}H_{n+n''}^{(1)}\left(k_r^{\text{ext}}D^i\right)J'_{n''}\left(k_r^{\text{ext}}R_{\text{ext}}\right)\\ &+\sum_{i<0}\alpha_{n''}^{i}H_{n+n''}^{(1)}\left(k_r^{\text{ext}}D^i\right)J'_{n''}\left(k_r^{\text{ext}}R_{\text{ext}}\right).\end{aligned} \tag{19}$$

From recognising the orthogonality of $\mathrm{e}^{\mathrm{j}n\varphi}$, applying a Fourier integral to both sides of the expression, and re-arranging the expression to determine the spectral coefficients for the external acoustic pressure ($\tilde{P}_n^{\text{ext}}$), we arrive at the following

$$\sum_{n''=-\infty}^{\infty}\Lambda'_{nn''}\tilde{P}_{n''}^{\text{ext}}\left(k_z\right) = \frac{\omega^2\rho_f^{\text{ext}}}{k_r^{\text{ext}}}\sum_{m=0}^{\infty}\tilde{W}_{mn}\tilde{X}_m\left(k_z\right), \tag{20}$$

with the Fourier transform of the mode shapes of a simply supported beam being [3]

$$\begin{aligned}\tilde{X}_m\left(k_z\right) &= \int_{-\infty}^{\infty}X_m\left(z\right)\mathrm{e}^{-\mathrm{j}k_z z}\,dz\\ &= \int_{-L}^{L}\cos\left(k_m z\right)\mathrm{e}^{-\mathrm{j}k_z z}\,dz\\ &= \begin{cases}\dfrac{2k_m\left(-1\right)^m\cos\left(k_z L\right)}{k_m^2-k_z^2} & \text{if } k_m \neq k_z,\\ L & \text{if } k_m = k_z.\end{cases}\end{aligned} \tag{21}$$

A truncation of the circumferential modes and axial modes are introduced, such that $n \in [-N, N]$ and $m \in [0, M]$, respectively

$$\sum_{n''=-N}^{N}\Lambda'_{nn''}\tilde{P}_{n''}^{\text{ext}} = \frac{\omega^2\rho_f^{\text{ext}}}{k_r^{\text{ext}}}\sum_{m=0}^{M}\tilde{W}_{mn}\tilde{X}_m\left(k_z\right). \tag{22}$$

The solution from the simultaneous equations will yield an expression that isolates the spectral external pressures

$$\sum_{n''=-N}^{N}\tilde{P}_{n''}^{\text{ext}} = \frac{\omega^2\rho_f^{\text{ext}}}{k_r^{\text{ext}}}\sum_{m=0}^{M}\sum_{n''=-N}^{N}\sum_{n'=-N}^{N}\overline{\Lambda}_{n''n'}\tilde{W}_{mn'}\tilde{X}_m\left(k_z\right), \tag{23}$$

where the terms $\overline{\Lambda}_{n''n'}$ can be practically determined by considering a matrix form of the formulation and taking an inversion of the corresponding term to $\Lambda'_{nn''}$. Substituting the spectral external pressures from Eq. (23) into Eq. (17), the fluid loading term can then be expressed as

$$\begin{aligned}f_l^{\text{ext}}\left(\varphi, z\right) &= \frac{1}{2\pi}\sum_{n=-N}^{N}\mathrm{e}^{\mathrm{j}n\varphi}\int_{-\infty}^{\infty}\sum_{m=0}^{M}\sum_{n'=-N}^{N}\left\{\sum_{n''=-N}^{N}\frac{\omega^2\rho_f^{\text{ext}}}{k_r^{\text{ext}}}\left(\Lambda_{nn''}\overline{\Lambda'}_{n''n'}\right)\right\}\tilde{W}_{mn'}\tilde{X}_m\left(k_z\right)\mathrm{e}^{\mathrm{j}k_z z}\,dk_z\\ &= \frac{1}{2\pi}\sum_{n=-N}^{N}\mathrm{e}^{\mathrm{j}n\varphi}\int_{-\infty}^{\infty}\sum_{m=0}^{M}\sum_{n'=-N}^{N}\tilde{Z}_{nn'}\left(k_z\right)\tilde{W}_{mn'}\tilde{X}_m\left(k_z\right)\mathrm{e}^{\mathrm{j}k_z z}\,dk_z,\end{aligned} \tag{24}$$

where we define the acoustic impedance as

$$\tilde{Z}_{nn'}\left(k_z\right) = \sum_{n''=-N}^{N}\frac{\omega^2\rho_f^{\text{ext}}}{k_r^{\text{ext}}}\Lambda_{nn''}\overline{\Lambda'}_{n''n'}. \tag{25}$$

It is recognised that there is a cross-modal coupling in the circumferential mode shapes embedded in this term. The coefficients for the external fluid loading $F_{l,mn}^{\text{ext}}$ are determined by applying the orthogonality relations from Eq. (4)

$$\tilde{F}_{l,mn}^{\text{ext}} = \frac{1}{L}\int_{-L}^{L}\frac{1}{2\pi}\int_{0}^{2\pi}\left\{\frac{1}{2\pi}\int_{-\infty}^{\infty}\sum_{n'=-N}^{N}\tilde{Z}_{nn'}\left(k_z\right)\sum_{m'=0}^{M}\tilde{W}_{m'n'}\tilde{X}_{m'}\left(k_z\right)\mathrm{e}^{\mathrm{j}k_z z}\,dk_z\right\}\mathrm{e}^{\mathrm{j}\left(n-n'\right)\varphi}X_m^*\left(z\right)\,d\varphi\,dz. \tag{26}$$

The right-hand side is re-arranged to identify the complex conjugate of the mode shapes in Fourier space $\tilde{X}_m^*\left(k_z\right) = \frac{1}{2\pi}\int_{-L}^{L}\int_{0}^{2\pi}X_m^*\left(z\right)\mathrm{e}^{\mathrm{j}k_z z}\,d\varphi\,dz$

$$\tilde{F}_{l,mn}^{\text{ext}} = \frac{1}{2\pi L}\int_{-\infty}^{\infty}\sum_{n'=-N}^{N}\tilde{Z}_{nn'}\left(k_z\right)\sum_{m'=0}^{M}\tilde{W}_{m'n'}\tilde{X}_{m'}\left(k_z\right)\tilde{X}_m^*\left(k_z\right)\,dk_z. \tag{27}$$

Therefore, the coefficients for the external fluid loading can be summarised with the following expression

$$\tilde{F}^{\text{ext}}_{l,mn} = \frac{1}{2\pi L}\sum_{m'=0}^{M}\sum_{n'=-N}^{N}\tilde{W}_{m'n'} \int_{-\infty}^{\infty}\tilde{Z}_{nn'}(k_z)\,\tilde{X}_{m'}(k_z)\,\tilde{X}^{*}_{m}(k_z)\,dk_z = \sum_{m'=0}^{M}\sum_{n'=-N}^{N}\tilde{Z}^{\text{ext}}_{mnm'n'}\tilde{W}_{m'n'}, \tag{28}$$

where we define the fluid loading impedance as [3, 38] $\tilde{Z}^{ext}_{mnm'n'} = \frac{1}{2\pi L}\int_{-\infty}^{\infty}\tilde{Z}_{nn'}(k_z)\,\tilde{X}_{m'}(k_z)\,\tilde{X}^{*}_{m}(k_z)\,dk_z$.

2.3 Internal Fluid Loading

2.3.1 Acoustic Propagation into the Internal Fluid

For the internal acoustic pressure, the Helmholtz equation is solved in a similar manner additionally considering that the pressure at the centre of the domain must be finite. The solution is known to take the general form [2]

$$p^{\text{int}}(r,\varphi,z) = \frac{1}{2\pi}\sum_{n=-\infty}^{\infty}\mathrm{e}^{\mathrm{j}n\varphi}\int_{-\infty}^{\infty}\tilde{P}^{\text{int}}_{n}(k_z)\,J_n\left(k_r^{\text{int}}r\right)\mathrm{e}^{\mathrm{j}k_z z}\,dk_z. \tag{29}$$

2.3.2 Internal Fluid-Shell Coupling

Similar to the external fluid-shell coupling, there is a continuity relation that is enforced at the interface between the inner surface of the shell and the internal fluid domain.

$$\left.\frac{\partial p^{\text{int}}}{\partial r}\right|_{r=R_{\text{int}}} = \begin{cases} -\omega^2\rho_f^{\text{int}}w, & |z|\le L,\\ 0, & |z|>L. \end{cases} \tag{30}$$

The radial displacement from Eq. (2) and internal acoustic pressures from Eq. (29) are substituted into Eq. (30) to obtain the following expression

$$\frac{k_r^{\text{int}}}{2\pi}\sum_{n=-\infty}^{\infty}\mathrm{e}^{\mathrm{j}n\varphi}\int_{-\infty}^{\infty}\tilde{P}^{\text{int}}_{n}(k_z)\,J'_n\left(k_r^{\text{int}}R_{\text{int}}\right)\mathrm{e}^{\mathrm{j}k_z z}\,dk_z = \omega^2\rho_f^{\text{int}}\sum_{n=-\infty}^{\infty}\mathrm{e}^{\mathrm{j}n\varphi}\sum_{m=0}^{\infty}\tilde{W}_{mn}X_m(z). \tag{31}$$

From recognising the orthogonality of $\mathrm{e}^{\mathrm{j}n\varphi}$, applying a Fourier integral to both sides of the expression, and rearranging the expression, the spectral coefficients for the external acoustic pressure are expressed as

$$\tilde{P}^{\text{int}}_{n}(k_z) = \frac{\omega^2\rho_f^{\text{int}}}{k_r^{\text{int}}J'_n\left(k_r^{\text{int}}R_{\text{int}}\right)}\sum_{m=0}^{\infty}\tilde{W}_{mn}\tilde{X}_m(k_z). \tag{32}$$

Internal fluid loading is then evaluated by substituting these spectral pressures into Eq. (29)

$$\begin{aligned} f_l^{\text{int}}(\varphi,z) &= p^{\text{int}}(r=R_{\text{int}},\varphi,z)\\ &= \frac{1}{2\pi}\sum_{n'=-\infty}^{\infty}\mathrm{e}^{\mathrm{j}n'\varphi}\int_{-\infty}^{\infty}\tilde{P}^{\text{int}}_{n'}(k_z)\,J_{n'}\left(k_r^{\text{int}}R_{\text{int}}\right)\mathrm{e}^{\mathrm{j}k_z z}\,dk_z\\ &= \frac{1}{2\pi}\sum_{n'=-\infty}^{\infty}\mathrm{e}^{\mathrm{j}n'\varphi}\int_{-\infty}^{\infty}\frac{\omega^2\rho_f^{\text{int}}}{k_r^{\text{int}}}\frac{J_{n'}\left(k_r^{\text{int}}R_{\text{int}}\right)}{J'_{n'}\left(k_r^{\text{int}}R_{\text{int}}\right)}\\ &\quad\sum_{m'=0}^{\infty}\tilde{W}_{m'n'}\tilde{X}_{m'}(k_z)\,\mathrm{e}^{\mathrm{j}k_z z}\,dk_z. \end{aligned} \tag{33}$$

The coefficients for the fluid loading can be evaluated by using the orthogonality relation from Eq. (4)

$$\begin{aligned} \tilde{F}^{\text{int}}_{l,mn} &= \frac{1}{L}\int_{-L}^{L}\frac{1}{2\pi}\int_{0}^{2\pi}\left\{\frac{1}{2\pi}\int_{-\infty}^{\infty}\frac{\omega^2\rho_f^{\text{int}}}{k_r^{\text{int}}}\frac{J_{n'}\left(k_r^{\text{int}}R_{\text{int}}\right)}{J'_{n'}\left(k_r^{\text{int}}R_{\text{int}}\right)}\right.\\ &\quad\left.\sum_{m'=0}^{\infty}\tilde{W}_{m'n'}\tilde{X}_{m'}(k_z)\,\mathrm{e}^{\mathrm{j}k_z z}\,dk_z\right\}\mathrm{e}^{\mathrm{j}(n'-n)\varphi}X^{*}_{m}(z)\,d\varphi\,dz\\ &= \frac{1}{2\pi L}\sum_{m'=0}^{\infty}\sum_{n'=-\infty}^{\infty}\tilde{W}_{m'n'}\int_{-\infty}^{\infty}\tilde{Z}^{\text{int}}_{nn'}(k_z)\,\tilde{X}_{m'}(k_z)\,\tilde{X}^{*}_{m}(k_z)\,dk_z\\ &= \sum_{m'=0}^{\infty}\sum_{n'=-\infty}^{\infty}\tilde{Z}^{\text{int}}_{mnm'n'}\tilde{W}_{m'n'}, \end{aligned} \tag{34}$$

where the internal radiation impedance is

$$\tilde{Z}^{\text{int}}_{nn'}(k_z) = \frac{\omega^2\rho_f^{\text{int}}}{k_r^{\text{int}}}\frac{J_n\left(k_r^{\text{int}}R_{\text{int}}\right)}{J'_n\left(k_r^{\text{int}}R_{\text{int}}\right)}\delta_{nn'}, \tag{35}$$

which shows there are no cross-modal coupling terms in the circumferential mode shapes and the internal fluid loading impedance [3, 38]

$$\tilde{Z}^{\text{int}}_{mnm'n'} = \frac{1}{2\pi L}\int_{-\infty}^{\infty}\tilde{Z}^{\text{int}}_{nn'}(k_z)\,\tilde{X}_{m'}(k_z)\,\tilde{X}^{*}_{m}(k_z)\,dk_z. \tag{36}$$

2.4 Vibroacoustic Equations of Motion

Returning to Eq. (6) and substituting the coefficients for the external fluid loading from Eq. (28) and internal fluid loading from Eq. (34) to obtain the following expression

$$\frac{\left|\tilde{\mathbf{L}}\right|}{\tilde{L}_{11}\tilde{L}_{22}-\tilde{L}_{12}\tilde{L}_{21}}\tilde{W}_{mn} + \gamma\sum_{m'=0}^{M}\sum_{n'=-N}^{N}\tilde{Z}_{mnm'n'}\tilde{W}_{m'n'} = \gamma\tilde{F}_{mn}, \tag{37}$$

where we the total fluid loading impedance is $\tilde{Z}_{mnm'n'} = \tilde{Z}^{\text{int}}_{mnm'n'} + \tilde{Z}^{\text{ext}}_{mnm'n'}$ to compact the expression. Once the coefficients for the radial displacements $\tilde{W}_{mn}$ are determined, it

Table 1 Dimensions and material properties of the shell and fluid properties

Parameter	Value
Young's Modulus E [GPa]	210
Poisson's ratio ν	0.3
Density of shell ρ_s [kg m^{-3}]	7850
Density of external fluid ρ_f^{ext} [kg m^{-3}]	1000
Density of internal fluid ρ_f^{int} [kg m^{-3}]	1000
Speed of sound of internal fluid $\bar{c}^{\text{ext}}$ [m s^{-1}]	1500
Speed of sound of internal fluid $\bar{c}^{\text{int}}$ [m s^{-1}]	1500
Thickness of shell h [mm]	50
Half-length L [mm]	5000
Mean radius R [mm]	1000
Structural damping η_s	0.01
Fluid damping η_f	0.001
Total depth H [m]	10
Distance to free surface H_{fs} [m]	5
Distance to rigid bottom H_{sb} [m]	5
Location of monopole source (r_s, φ_s, z_s) [m, rad, m]	(0.5, 0, 0)
Location of point load (φ_f, z_f) [rad, m]	(0, 0)

can then be substituted into the fluid–structure coupling equation from Eq. (20) to determine the spectral external acoustic pressures. The external acoustic pressure is then evaluated by Eq. (8) by considering the image-source real-source relation $\tilde{P}_n^{\text{ext},i} = \alpha_n^i \tilde{P}_n^{\text{ext}}$ [24, 26].

2.5 Excitation of the Shell

In the vibroacoustic equation of Eq. (37), the remaining term to define is the input radial forcing term f_e, and more specifically its corresponding coefficient $\tilde{F}_{mn}$ after applying the orthogonality relations of Eq. (4). In the system of interest, two types of excitations are considered: a mechanical point load and an acoustic monopole source.

2.5.1 Mechanical Point Load

For a mechanical point load applied at a location on the inner surface of the shell $(R_{\text{int}}, \varphi_f, z_f)$, the general expression is

$$f_e = \frac{F_0}{R_{\text{int}}} \delta(\varphi - \varphi_f)\, \delta(z - z_f), \tag{38}$$

and its coefficients after decomposing into m, n modes are

$$\tilde{F}_{mn} = \frac{F_0}{2\pi R_{\text{int}} L} e^{-jn\varphi_f} X_m(z_f). \tag{39}$$

2.5.2 Acoustic Monopole Source

Radiated acoustic pressure from an internal monopole source located at $(R_{\text{int}}, \varphi_s, z_s)$ is given as [39, 40]

$$f_e = \begin{cases} \displaystyle\sum_{n=-\infty}^{\infty} e^{jn\varphi} \int_{-\infty}^{\infty} \left\{ \frac{j\omega\rho_f}{4} \frac{J_n(k_r r_s)}{J_n'(k_r R_{\text{int}})} \left[J_n(k_r r)\, Y_n'(k_r R_{\text{int}}) \right.\right. \\ \left.\left. - J_n'(k_r R_{\text{int}})\, Y_n(k_r r) \right] e^{-jn\varphi_s} e^{-jk_z z_s} \right\} e^{jk_z z}\, dk_z \\ \text{for } r > r_s, \\ \displaystyle\sum_{n=-\infty}^{\infty} e^{jn\varphi} \int_{-\infty}^{\infty} \left\{ \frac{j\omega\rho_f}{4} \frac{J_n(k_r r)}{J_n'(k_r R_{\text{int}})} \left[J_n(k_r r_s)\, Y_n'(k_r R_{\text{int}}) \right.\right. \\ \left.\left. - J_n'(k_r R_{\text{int}})\, Y_n(k_r r_s) \right] e^{-jn\varphi_s} e^{-jk_z z_s} \right\} e^{jk_z z}\, dk_z \\ \text{for } r < r_s. \end{cases} \tag{40}$$

The forcing term required is the blocked pressure at the inner surface of the shell (i.e. $r = R_{\text{int}} > r_s$) and is obtained from applying a Wronskian relation [41] to Eq. (40)

$$f(\varphi, z) = \sum_{n=-\infty}^{\infty} e^{jn\varphi} \int_{-\infty}^{\infty} \left\{ \frac{j\omega\rho_f}{2\pi k_r R_{\text{int}}} \frac{J_n(k_r r_s)}{J_n'(k_r R_{\text{int}})} e^{-jn\varphi_s} e^{-jk_z z_s} \right\} e^{jk_z z}\, dk_z. \tag{41}$$

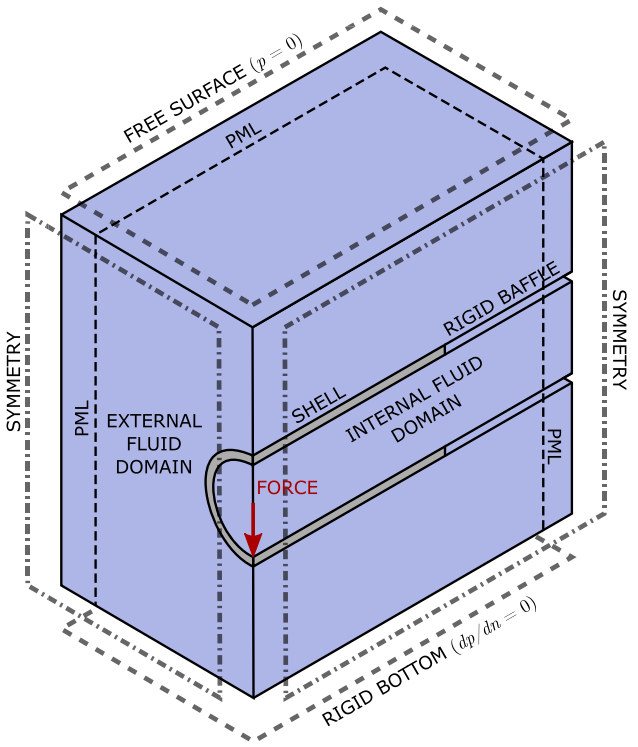

Fig. 2 Schematic of the finite element model of the baffled shell in an underwater waveguide

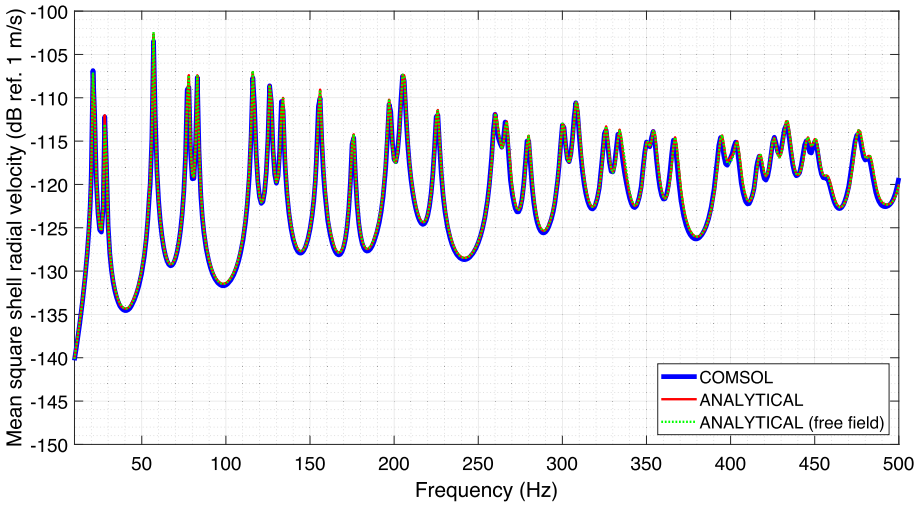

(a) Point load.

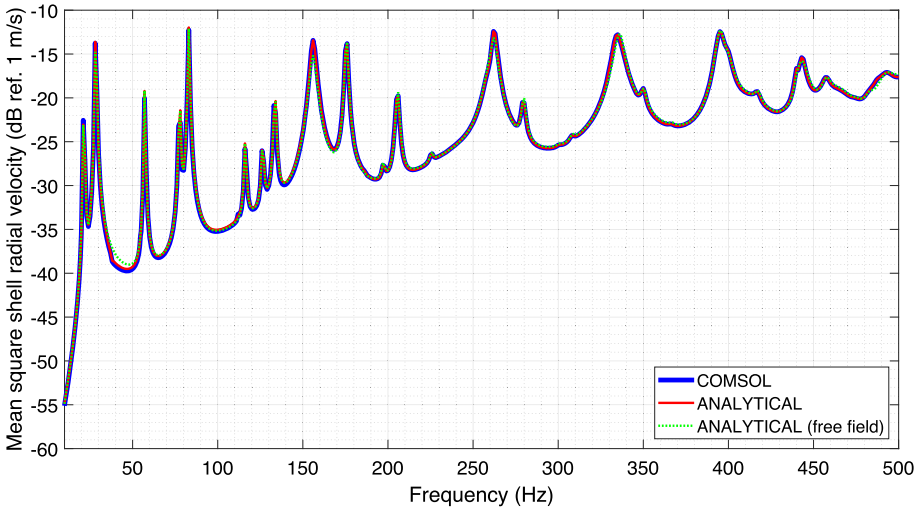

(b) Monopole source.

Fig. 3 Mean square shell radial velocity for an excited shell in a fluid domain of an acoustic waveguide from an analytical solution (ANALYTICAL) and equivalent FE model (COMSOL)

The corresponding force coefficients are

$$\tilde{F}_{mn} = \frac{1}{2\pi L}\int_{-L}^{L}\int_{-\infty}^{\infty}\left\{\frac{\mathrm{j}\omega\rho_f}{2\pi k_r R_{\text{int}}}\frac{J_n(k_r r_s)}{J_n'(k_r R_{\text{int}})}\mathrm{e}^{-\mathrm{j}n\varphi_s}\mathrm{e}^{-\mathrm{j}k_z z_s}\right\} X_m(z)\, dk_z\, dz = \frac{1}{2\pi L}\int_{-\infty}^{\infty}\left\{\frac{\mathrm{j}\omega\rho_f}{2\pi k_r R_{\text{int}}}\frac{J_n(k_r r_s)}{J_n'(k_r R_{\text{int}})}\mathrm{e}^{-\mathrm{j}n\varphi_s}\mathrm{e}^{-\mathrm{j}k_z z_s}\right\}\tilde{X}_m^*(k_z)\, dk_z. \quad (42)$$

2.6 Vibroacoustic Indicators

Two vibroacoustic indicators are evaluated which include the mean square radial velocity of the shell given by the following expression

$$\langle v\rangle^2(\omega) = \frac{1}{S}\int_S |-\mathrm{j}\omega w(\varphi, z)|^2\, dS = \frac{\omega^2}{2}\sum_{m=0}^{M}\sum_{n=-N}^{N}\left|\tilde{W}_{mn}\right|^2, \quad (43)$$

and the radiated sound power to the external environment is evaluated by taking the surface integral of the active component of the acoustic intensity at the surface of the shell

$$\Pi(\omega) = \frac{1}{2}\int_S \text{Real}\left\{f_l^{\text{ext}}(\varphi, z)\cdot \mathrm{j}\omega w^*(\varphi, z)\right\} dS \quad (44)$$

$$= \frac{S}{4}\text{Real}\left\{\sum_{m=0}^{M}\sum_{n=-N}^{N}\sum_{m'=0}^{M}\sum_{n'=-N}^{N}\mathrm{j}\omega\tilde{Z}_{mnm'n'}\tilde{W}_{m'n'}\tilde{W}_{mn}^*\right\}, \quad (45)$$

where Real{ } denotes taking the real part of the value, and in this case, the active component of intensity.

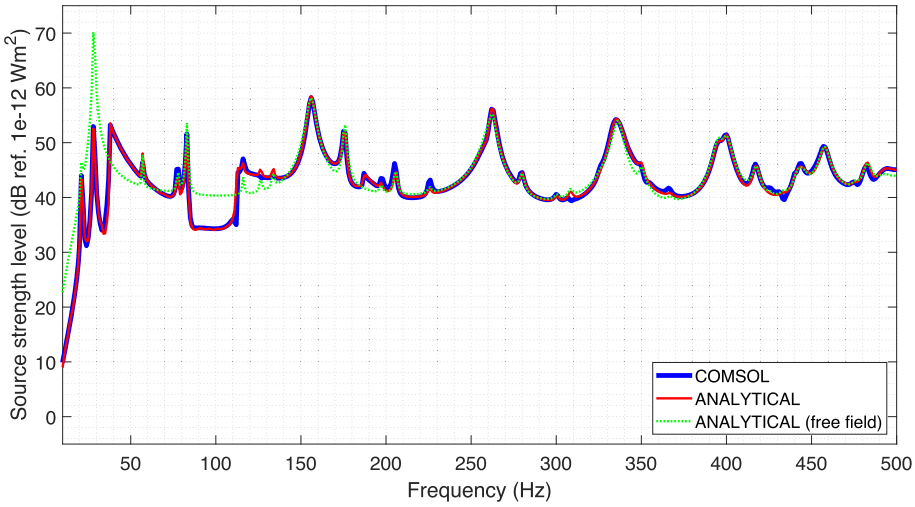

(a) Point load.

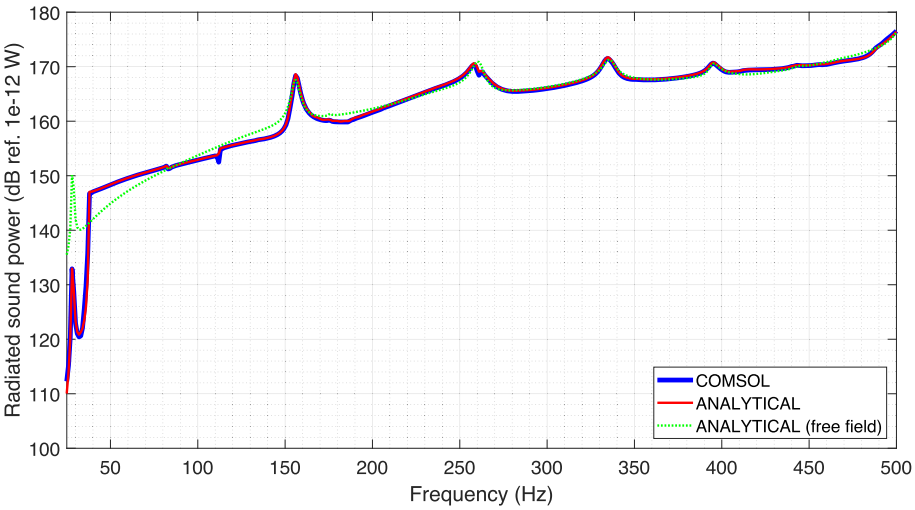

(b) Monopole source.

Fig. 4 Radiated sound power for an excited shell in a fluid domain of an acoustic waveguide from an analytical solution (COMSOL) and equivalent FE model (COMSOL)

3 Numerical Results

The proposed analytical approach is implemented with MATLAB with the following numerical example that is specified in Table 1. Both the vibration response and the acoustic response are predicted with the present approach and compared against an equivalent model using the FEM in COMSOL Multiphysics v6.1. For the analytical framework, the number of image sources is found to achieve numerical convergence with a truncation of $i \in [-300, 300]$. The integration over axial wavenumbers is performed numerically via a rectangle rule. The Gaussian quadrature scheme can also be employed with marginal improvements in runtime. The maximum circumferential mode order $n \in [-N, N]$ to consider is based on a criterion $N = \text{ceil}\left[1.5 \times R_{\text{ext}} \max\left(k, k_p^{fl}\right) + 1\right]$ [42], where ceil ( ) is the ceiling function, $k_p^{fl} \approx \left[k_p^4 + \omega^2 \rho_f / \left(D\sqrt{k_p^2 - k^2}\right)\right]^{1/4}$ is the flexural wavenumber of an equivalent fluid-loaded plate, and k_p is the flexural wavenumber of an in-vacuo plate. The maximum axial mode order is found to be sufficient for $M = \text{ceil}\,(2L)$. There are many parameters involved in the vibroacoustic system at hand, of which some of the important phenomena have already been investigated previously. For example, it was shown that a fully coupled analytical model is important rather than using typical mirror effect model [24, 26] to model the underwater acoustics of the cylindrical shell. Additionally, far-field acoustic pressures were investigated for varying waveguide depths which demonstrated a stronger influence when in proximity to a seafloor compared to the sea surface.

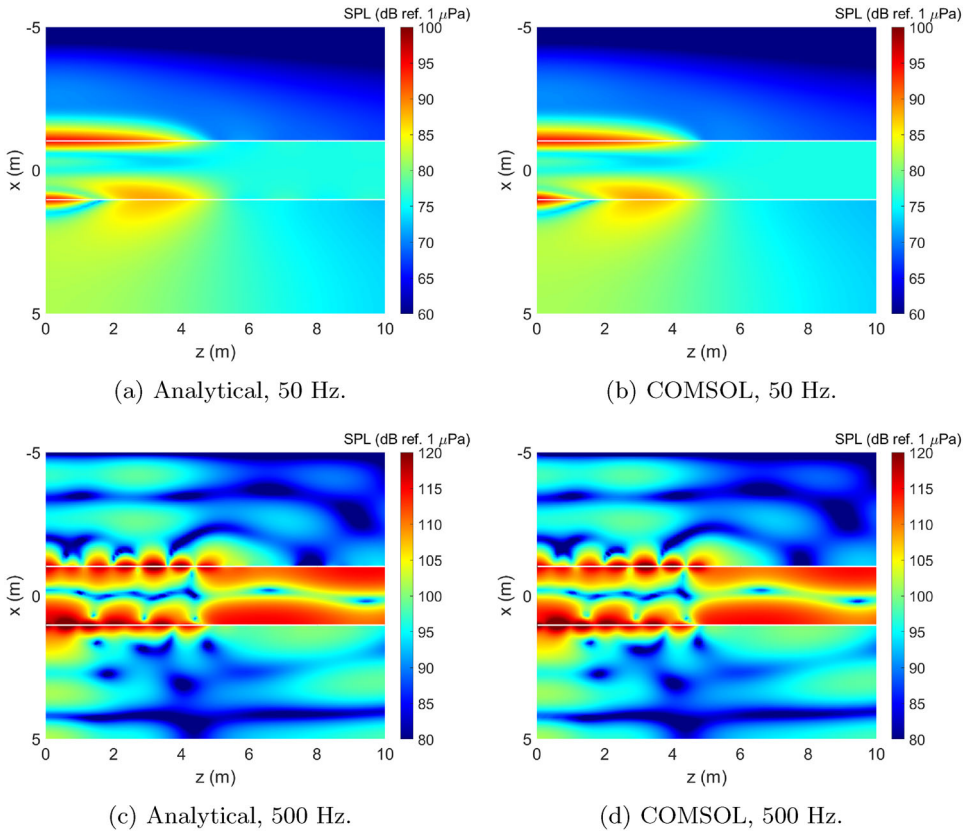

Fig. 5 Acoustic pressure contours in the $x-z$ plane ($y=0$) for a point-load-excited shell

First, verification of the analytical approach is demonstrated by comparison of predicted vibroacoustic responses with a specific numerical example against an equivalent finite element model using COMSOL Multiphysics. A schematic of the finite element model is shown in Fig 2. Symmetry planes reduce the computational domain to a quarter domain with an excitation that is applied in the mid-plane of the shell due to a symmetry in the $x-y$ and $x-z$ planes. The external fluid domain is terminated by a pressure release condition ($p=0$), and a lower rigid bottom ($\partial p/\partial n = 0$, where n is the normal direction), and the remaining faces are extended by a perfectly matched layer to simulate the Sommerfeld radiation condition (infinitely outgoing waves). The internal fluid domain is terminated by PML. Structured mesh is employed in the PMLs to ensure numerical convergence. The vibroacoustic system is separated into two components: the finite cylindrical shell, modelled with the Solid Mechanics module, and the fluid domains (external and internal), modelled with the Pressure Acoustics module. At the interfaces between these two components is a coupling via the Multiphysics module, acoustic-structure boundary. Also, at the ends of the cylindrical shell is a simply supported boundary condition, in which the in-plane displacements are set to be zero while the out-of-plane displacement is free. The fluid domain is then discretised with a fine mesh to ensure at least twelve elements per wavelength. Comparison against the analytical solution is made by evaluating vibroacoustic indicators of interest, which includes the mean square radial velocity of the shell, radiated sound power, and acoustic pressures received in the external fluid domain of an ideal shallow waveguide.

Mean square radial velocity of the shell is evaluated using Eq. (43). Only the rigorous computation of the modal displacement $\tilde{W}_{mn}$ is necessary for its evaluation. Therefore, only the vibroacoustic equations of motion of Eq. (37) are solved. For the finite element model (COMSOL), a surface average of the square radial velocity of the shell yields the desired calculation. The comparison is shown in Fig. 3 and demonstrates excellent agreement between the analytical solution and the equivalent finite element model. This verifies the structural component of the vibroacoustic system. When compared to the analytical solution with the surrounding fluid domain of an acoustic free field instead, the results are unchanged. This is expected as the fluid domain will only affect the acoustic modes (low values of n), which will not appear in the vibration response that is dominated by structural modes (higher values of n).

Radiated sound power is evaluated using Eq. (44). The expression indicates that two terms are necessary for its eval-

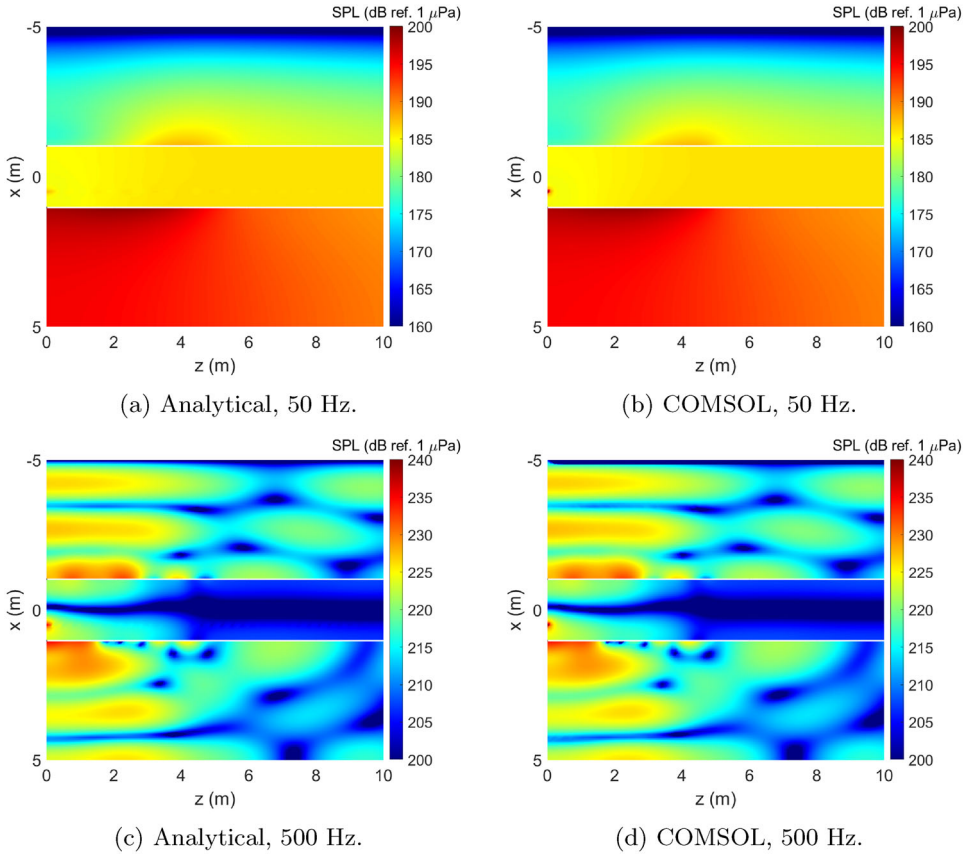

Fig. 6 Acoustic pressure contours in the $x-z$ plane ($y=0$) for a monopole source-excited shell

uation, the external fluid loading impedance $\tilde{Z}_{mnm'n'}$ and modal displacement $\tilde{W}_{mn}$, while, for the finite element model (COMSOL), the surface integral of active acoustic intensity Real$\{I_a\}$ projected onto the normal direction $\hat{n}$ provides the necessary calculation

$$\Pi(\omega) = \frac{1}{2}\int_S \text{Real}\left\{I_a \cdot \hat{n}\right\} dS. \tag{46}$$

This is equivalent to Eq. (44) and can be used for the calculation instead. At very low frequencies ($<$ 10 Hz for the point load excitation and $<$ 25 Hz for the monopole source excitation), the values of radiated sound power are very low. Therefore, it is omitted to maintain a reasonable dynamic range, which is chosen to be 80 dB. The comparison is shown in Fig. 4 and is in good agreement. As the radiated sound power incorporates the fluid loading impedance, it verifies the vibroacoustic fluid–structure coupling of the system. Furthermore, the radiated sound power is compared against the analytical solution for a shell in an acoustic free field. It is observed that the waveguide fluid domain influences the low-frequency aspects of the radiated sound power. It is mentioned that the analytical model is at least three times faster than the corresponding finite element model for a shell in a shallow waveguide and becomes much more efficient in the analysis of shells in larger waveguide fluid domains that eventually become computationally impractical for the FEM.

Furthermore, acoustic pressures in the internal and external fluid domains are evaluated to verify the predicted internal acoustic behaviour and external acoustic propagation in an ideal shallow waveguide. Acoustic pressure is presented as a sound pressure level (SPL), SPL $= 20\log_{10}(|p|/p_{\text{ref}})$ where $p_{\text{ref}} = 10^{-6}$ Pa. First, the acoustic pressure contours at a low excitation frequency of 50 Hz and high excitation frequency of 500 Hz are presented for a point-load-excited shell in Fig. 5 and monopole source-excited shell in Fig. 6. The acoustic pressure contour in the $x-z$ ($y=0$) plane, covering a 10×10 m^2 region, is shown in Figs. 5 and 6. It is shown that the comparison against the equivalent finite element model is in excellent agreement. It is also highlighted that for the monopole excitation, the total acoustic pressure within the internal fluid domain of the shell corresponds to the sum of the acoustic pressure induced directly by the monopole, f_e (see Eq. (40)) and the radiated acoustic pressure due to the elastic deformations of the shell p^{int} (see Eq. (29)).

An acoustic pressure spectrum is presented in Fig. 7 to supplement the acoustic pressure contours. The external acoustic

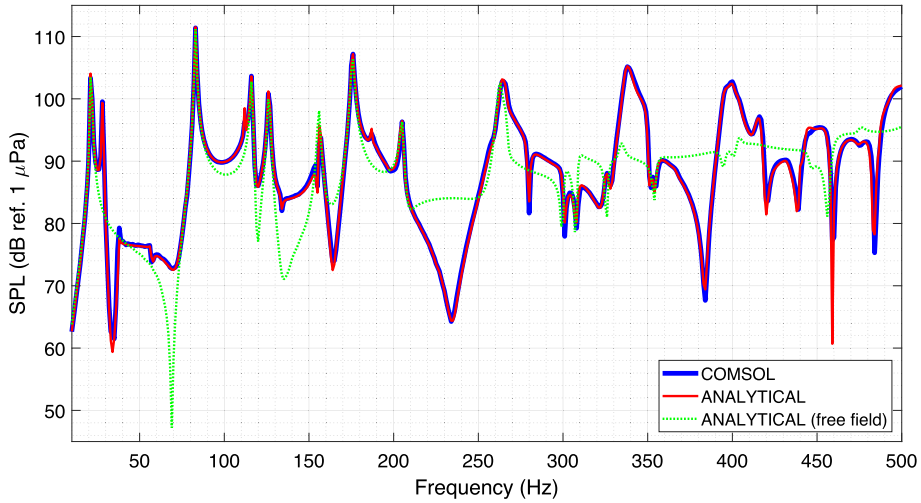

(a) Point load.

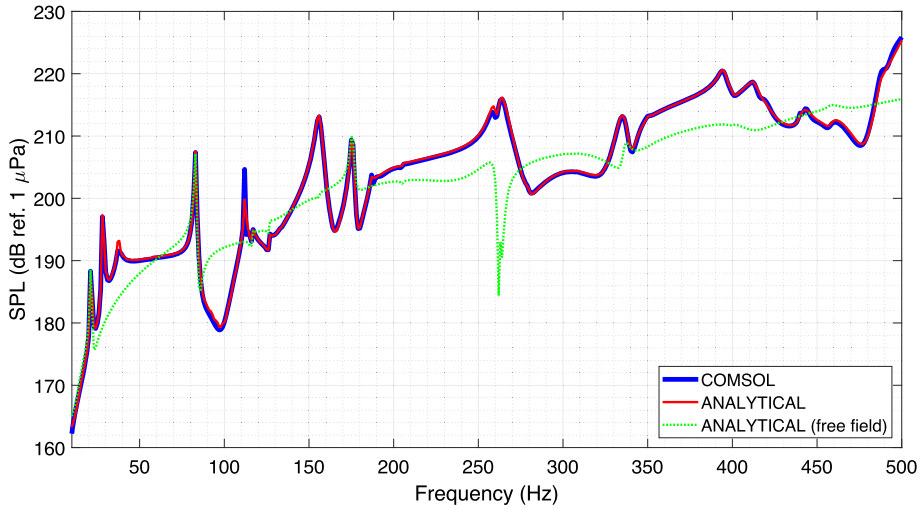

(b) Monopole source.

Fig. 7 Acoustic pressure received at a point ($r = R + 1, \varphi = \pi/2, z = 0$)

pressure is received at a point in the plane of excitation ($z = 0$), 1 m from the surface of the shell ($r = R + 1$ m) and parallel to the acoustic boundaries ($\varphi = \pi/2$). The comparison is made for both a point-load-excited shell and monopole source-excited shell. Excellent agreement is observed across the excitation frequencies between 10 Hz and 500 Hz. The acoustic pressure received in an acoustic free field is generally very different to that of a waveguide fluid domain due to the influence of the acoustic boundaries (pressure release and rigid floor). Even though the acoustic pressure is distributed differently in a waveguide fluid domain, the radiated sound power is relatively unaffected, only at the low frequency range ($<$ 250 Hz) Fig. 4) there is a significant difference. Therefore, for the subsequent investigation into the influence of the acoustic boundaries, the analysis is limited to the low frequency portion of the radiated sound power.

Finally, an investigation into the effect of fluid domains on the low frequency radiated sound power ($<$ 250 Hz) is presented here. In Fig. 8, we see a comparison against the waveguide depths for a shell positioned at the midpoint. Increasing the waveguide depth to 100 m is sufficient for the radiated sound power to approximate the shell in an acoustic free field, which is equivalent to setting the number of images to 0, while reducing the waveguide depth to 5 m reduces the radiated sound power at the lower end of the spectrum. At higher frequencies, it is observed that the power tends to be similar to that of a shell in an acoustic free field. Now the centre of the shell is positioned at 2.5 m from the free surface in Fig. 9 and at 2.5 m from the rigid bottom in Fig. 10. In a waveguide fluid domain of 10 m, the shell is then closer to the free surface in Fig. 9, and closer to the rigid floor in Fig. 10. To provide a point of comparison, sound power calculations

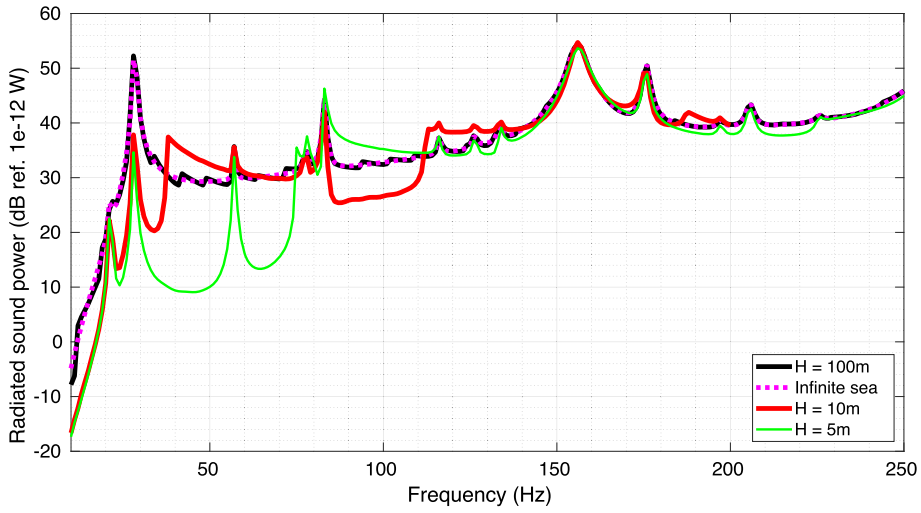

(a) Point load.

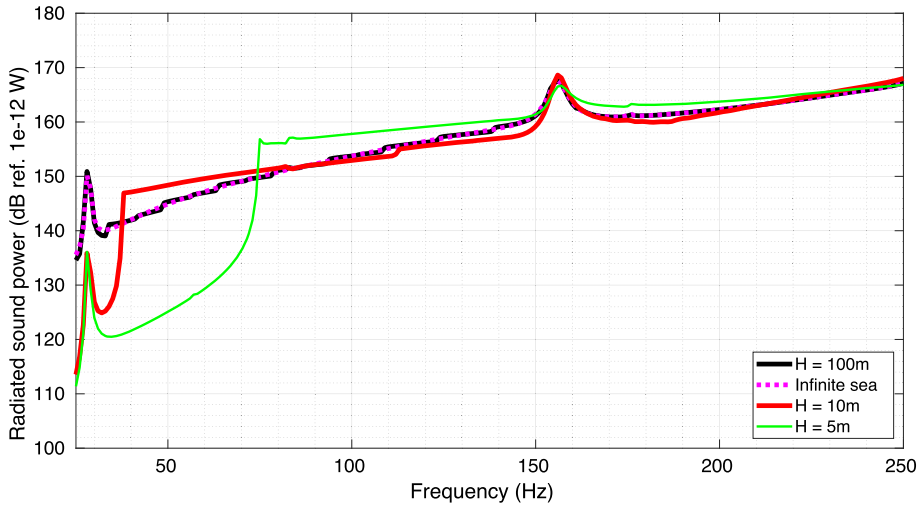

(b) Monopole source.

Fig. 8 Radiated sound power at the low frequency range for a shell positioned in the middle of different waveguide depths

are performed for a shell in a semi-infinite acoustic domain (acoustic half-space) that is bounded by either a free surface or rigid bottom (at 2.5 m from the centre of the shell) and the results are shown, respectively, in Figs. 9 and 10. It is noticed that increasing the total waveguide depth to 100 m will result in the radiated sound power approximating to the corresponding acoustic half-space case, which is equivalent to setting the number of images to either 1 upper image only for the free surface only case or 1 lower image only for the rigid bottom only case. It can then be inferred from these results that at reasonable waveguide depths, the radiated sound power in both the low and higher frequency range can be approximated by the corresponding limiting case. However, for very shallow waveguides, for instance $H = 10$ m, it is important to incorporate the influence of the acoustic boundaries, especially at the low frequency range.

4 Conclusions

An analytical framework for the vibroacoustic behaviour of a baffled finite-length thin elastic fluid-filled cylindrical shell that is held by infinitely long rigid baffles and submerged in an ideal shallow-water waveguide is herein presented. The analysis involves combining the governing equations from thin shell theory with the acoustic pressures from the Helmholtz equation and image-source method to capture the interaction with a shallow-water waveguide. Compared to previous formulations of a two-dimensional shell (i.e. an infinitely long cylindrical shell that is excited by an infinite line force) and a three-dimensional infinitely long shell, there is a similar phenomenon of cross-modal coupling in the circumferential mode orders as found in analytical expressions with indexing of nn'. However, with the addition of a finite elastic region,

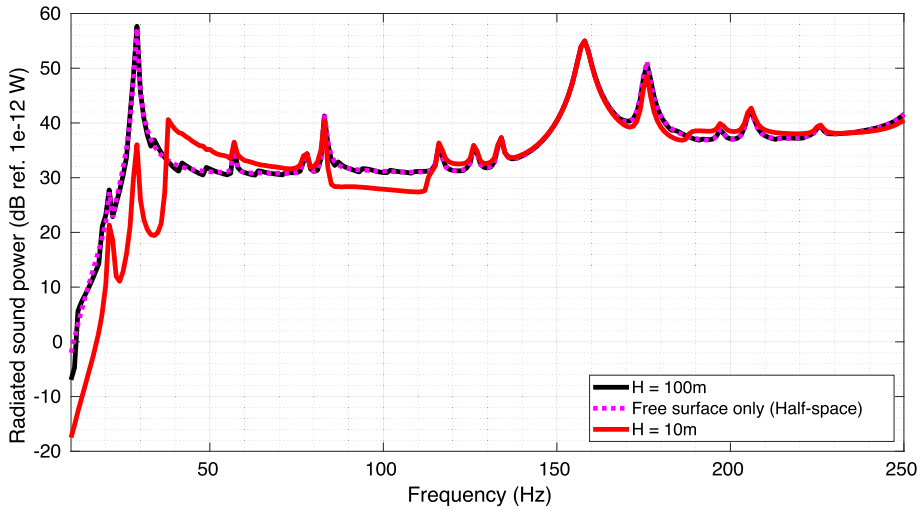

(a) Point load.

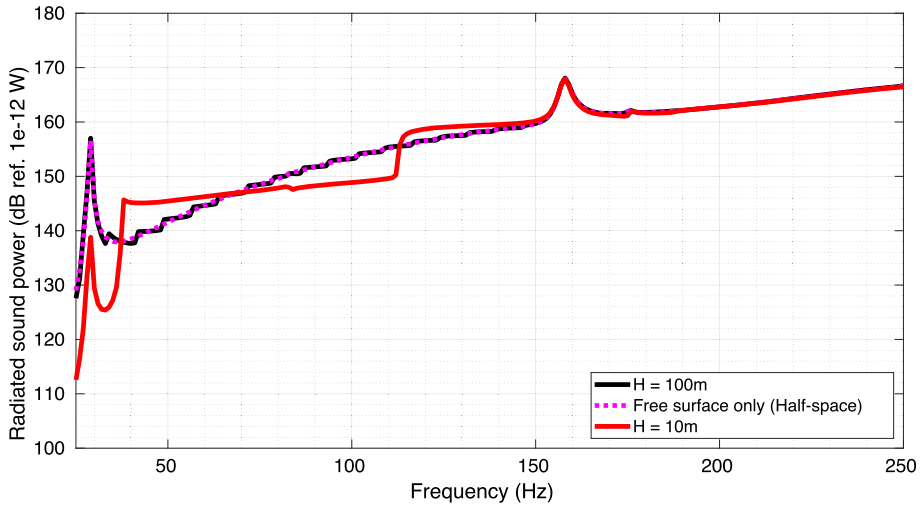

(b) Monopole source.

Fig. 9 Radiated sound power at the low frequency range for a shell positioned in $H_{fs} = 2.5$ m from the free surface of two different waveguide depths ($H = 10, 100$ m)

there is an additional cross-modal coupling in the axial modes (i.e. an indexing of mm'). A fully coupled vibroacoustic equation is then derived from the fluid–structure coupling between the external shallow-water waveguide fluid domain, internal cylindrical fluid domain and excited baffled thin elastic shell structure, where the excitation is specified either as a mechanical point load or from the radiated pressures from an internal acoustic monopole source. Using a numerical example, the analytical model is verified against an equivalent model that is generated using the FEM with COMSOL Multiphysics v6.1. The analytical model is at least three times faster than the corresponding finite element model and is capable of evaluating large waveguide fluid domains that become computationally impractical for the FEM. Vibration and acoustic responses are compared for verification and comparison against a shell submerged in an acoustic free field (infinite sea). It is observed that the pressure distribution within the fluid domain is very different for the case of a waveguide and an acoustic free field due to the interaction with the waveguide boundaries. However, when comparing the radiated sound power, it is mainly affected at the low frequency range. Different waveguide depths were investigated using the analytical model. For different fluid domains, it was demonstrated that waveguide depths of 100 m approximate the free field power. When the shell was shifted to bias one acoustic boundary, the influence of the opposing acoustic boundary on the radiated sound power was also negligible at

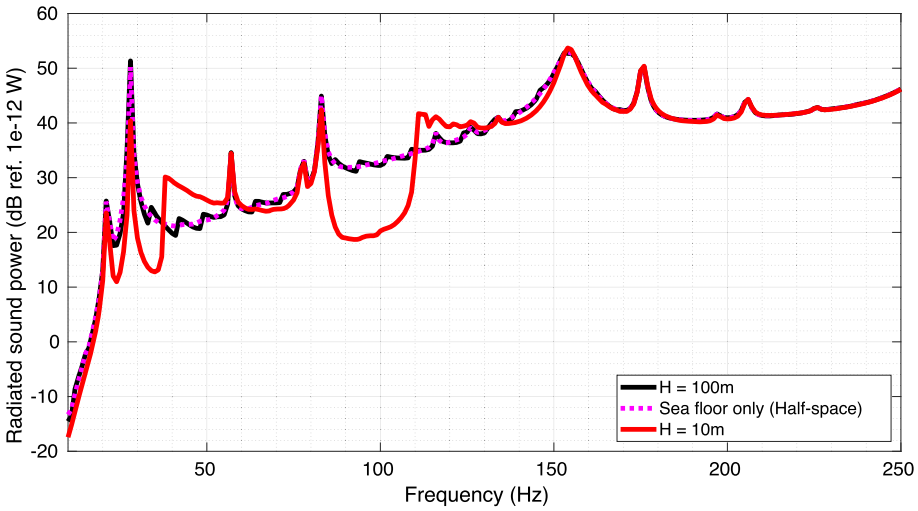

(a) Point load.

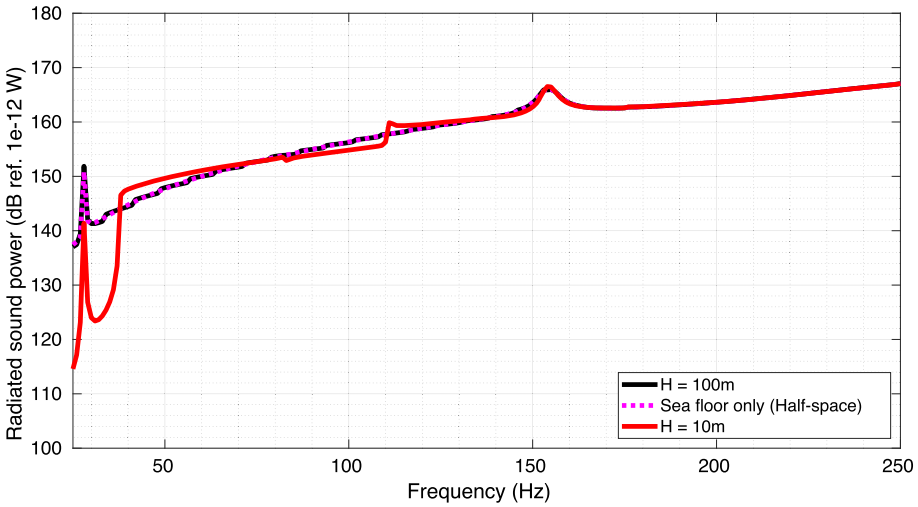

(b) Monopole source.

Fig. 10 Radiated sound power at the low frequency range for a shell positioned in $H_{sb} = 2.5$ m from the rigid floor of two different waveguide depths ($H = 10, 100$ m)

reasonable distances and can be approximated by the corresponding acoustic half-space.

Funding Open Access funding enabled and organized by CAUL and its Member Institutions The authors did not receive support from any organization for the submitted work.

Declarations

Conflict of interest The authors declare that they have no Conflict of interest.

References

1. Leissa, A.W.: Vibration of Shells. American Institute of Physics, Washington, D.C. (1993)
2. Williams, E.G.: Fourier Acoustics: Sound Radiation and Nearfield Acoustical Holography. Academic Press, London (1999)

3. Junger, M.C., Feit, D.: Sound, Structures, and Their Interaction. MIT Press, Cambridge (1986)
4. Skelton, E.A., James, J.H.: Theoretical Acoustics of Underwater Structures. Imperial College Press, London (1997)
5. Pathak, A.G., Stepanishen, P.R.: Acoustic harmonic radiation from fluid-loaded infinite cylindrical elastic shells using elasticity theory. J. Acoust. Soc. Am. **96**(1), 573–582 (1994). https://doi.org/10.1121/1.410443
6. Guo, Y.P.: Acoustic scattering from cylindrical shells with deck-type internal plate at oblique incidence. J. Acoust. Soc. Am. **99**(5), 2701–2713 (1996). https://doi.org/10.1121/1.414812
7. Liu, Z., Li, T., Zhu, X., Zhang, J.: The effect of hydrostatic pressure fields on the dispersion characteristics of fluid-shell coupled system. J. Mar. Sci. App. **9**(2), 129–136 (2010). https://doi.org/10.1007/s11804-010-9010-3
8. Kerferd, B., Eggler, D., Karimi, M., Kessissoglou, N.: Active acoustic cloaking of cylindrical shells in low mach number flow. J. Sound Vib. **479**, 115400 (2020). https://doi.org/10.1016/j.jsv.2020.115400
9. Maxit, L., Karimi, M., Meyer, V., Kessissoglou, N.: Vibroacoustic responses of a heavy fluid loaded cylindrical shell excited by a turbulent boundary layer. J. Fluids Struc. **92**, 102758 (2020). https://doi.org/10.1016/j.jfluidstructs.2019.102758
10. Maxit, L., Karimi, M., Guasch, O.: Spatial coherence of pipe vibrations induced by an internal turbulent flow. J. Sound Vib. **493**, 115841 (2021)
11. Williams, P., Kirby, R., Karimi, M.: Sound power radiated from acoustically thick, fluid loaded, axisymmetric pipes excited by a central monopole. J. Sound Vib. **527**, 116843 (2022). https://doi.org/10.1016/j.jsv.2022.116843
12. Salaün, P.: Effect of a free surface on the far-field pressure radiated by a point-excited cylindrical shell. J. Acoust. Soc. Am. **90**(4), 2173–2181 (1991). https://doi.org/10.1121/1.402373
13. Ergin, A., Temarel, P.: Free vibration of a partially liquid-filled and submerged, horizontal cylindrical shell. J. Sound Vib. **254**(5), 951–965 (2002). https://doi.org/10.1006/jsvi.2001.4139
14. Li, H.L., Wu, C.J., Huang, X.Q.: Parametric study on sound radiation from an infinite fluid-filled/semi-submerged cylindrical shell. Appl. Acoust. **64**(5), 495–509 (2003). https://doi.org/10.1016/S0003-682X(02)00125-1
15. Guo, W., Li, T., Zhu, X., Miao, Y., Zhang, G.: Vibration and acoustic radiation of a finite cylindrical shell submerged at finite depth from the free surface. J. Sound Vib. **393**, 338–352 (2017). https://doi.org/10.1016/j.jsv.2017.01.003
16. Zhao, K., Fan, J., Wang, B., Tang, W.: Vibroacoustic behavior of a partially immersed cylindrical shell under point-force excitation: analysis and experiment. Appl. Acoust. **161**, 107170 (2020). https://doi.org/10.1016/j.apacoust.2019.107170
17. Hasheminejad, S.M., Azarpeyvand, M.: Modal vibrations of an infinite cylinder in an acoustic halfspace. Int. J. Eng. Sci. **41**(19), 2253–2271 (2003). https://doi.org/10.1016/S0020-7225(03)00214-3
18. Hasheminejad, S.M., Azarpeyvand, M.: Modal vibrations of a cylindrical radiator over an impedance plane. J. Sound Vib. **278**(3), 461–477 (2004). https://doi.org/10.1016/j.jsv.2003.10.039
19. Li, T.Y., Miao, Y.Y., Ye, W.B., Zhu, X., Zhu, X.M.: Far-field sound radiation of a submerged cylindrical shell at finite depth from the free surface. J. Acoust. Soc. Am. **136**(3), 1054–1064 (2014). https://doi.org/10.1121/1.4890638
20. Marsick, A., Sharma, G.S., Eggler, D., Maxit, L., Meyer, V., Kessissoglou, N.: On the vibro-acoustic response of a cylindrical shell submerged near a free sea surface. J. Sound Vib. **511**, 116359 (2021). https://doi.org/10.1016/j.jsv.2021.116359
21. Caresta, M., Kessissoglou, N.J.: Acoustic signature of a submarine hull under harmonic excitation. Appl. Acoust. **71**(1), 17–31 (2010). https://doi.org/10.1016/j.apacoust.2009.07.008
22. Jiang, L., Zou, M., Huang, H., Feng, X.: Integrated calculation method of acoustic radiation and propagation for floating bodies in shallow water. J. Acoust. Soc. Am. **143**(5), 430–436 (2018). https://doi.org/10.1121/1.5039415
23. Jiang, L.-W., Zou, M.-S., Liu, S.-X., Huang, H.: Calculation method of acoustic radiation for floating bodies in shallow sea considering complex ocean acoustic environments. J. Sound Vib. **476**, 115330 (2020). https://doi.org/10.1016/j.jsv.2020.115330
24. Kha, J., Karimi, M., Maxit, L., Skvortsov, A., Kirby, R.: Forced vibroacoustic response of a cylindrical shell in an underwater acoustic waveguide. Ocean Eng. **273**, 113899 (2023). https://doi.org/10.1016/j.oceaneng.2023.113899
25. Dumortier, F., Kha, J., Karimi, M., Meyer, V., Maxit, L.: A subtractive modelling approach for predicting the radiation of a cylindrical shell in a waveguide. Acta Acustica **9**, 29 (2025)
26. Kha, J., Karimi, M., Maxit, L., Kirby, R.: Near-and far-field radiated acoustic pressures from a vibrating three-dimensional cylindrical shell in an underwater acoustic waveguide. J. Sound Vib. **8**, 118534 (2024)
27. Guo, Y., Wang, H., Yi, H.: Vibration and sound radiation of submerged finite cylindrical shells with pre-stress. Sci. Rep. **9**(1), 11307 (2019)
28. Guo, W., Hong, X., Han, Y., Li, T., Zhu, X.: Vibration and far-field sound radiation of a horizontal, finite-long cylindrical shell partially submerged in fluid. Arch. Appl. Mech. **93**(4), 1491–1505 (2023). https://doi.org/10.1007/s00419-022-02341-9
29. Sandman, B.: Fluid-loading influence coefficients for a finite cylindrical shell. J. Acoust. Soc. Am. **60**(6), 1256–1264 (1976)
30. Laulagnet, B., Guyader, J.: Modal analysis of a shell's acoustic radiation in light and heavy fluids. J. Sound Vib. **131**(3), 397–415 (1989)
31. Meyer, V., Maxit, L., Guyader, J.-L., Leissing, T.: Prediction of the vibroacoustic behavior of a submerged shell with non-axisymmetric internal substructures by a condensed transfer function method. J. Sound Vib. **360**, 260–276 (2016)
32. Dumortier, F., Meyer, V., Maxit, L.: Scattering from a partially coated shell immersed in water using a subtractive modelling technique. J. Theor. Comput. Acoust. **31**(04), 2350020 (2023). https://doi.org/10.1142/S2591728523500202
33. Chen, L., Liang, X., Yi, H.: Vibro-acoustic characteristics of cylindrical shells with complex acoustic boundary conditions. Ocean Eng. **126**, 12–21 (2016). https://doi.org/10.1016/j.oceaneng.2016.08.028
34. Guo, W., Li, T., Zhu, X., Miao, Y.: Sound-structure interaction analysis of an infinite-long cylindrical shell submerged in a quarter water domain and subject to a line-distributed harmonic excitation. J. Sound Vib. **422**, 48–61 (2018). https://doi.org/10.1016/j.jsv.2018.02.031
35. Wang, P., Li, T., Zhu, X.: Free flexural vibration of a cylindrical shell horizontally immersed in shallow water using the wave propagation approach. Ocean Eng. **142**, 280–291 (2017). https://doi.org/10.1016/j.oceaneng.2017.07.006
36. Zhang, L., Duan, J., Da, L., Xu, G., Sun, X.-H.: Vibroacoustic radiation and propagation properties of slender cylindrical shell in uniform shallow sea. Ocean Eng. **195**, 106659 (2020). https://doi.org/10.1016/j.oceaneng.2019.106659
37. Baynes, A.B.: Scattering of low-frequency sound by compact objects in underwater waveguides. PhD thesis, Monterey, CA; Naval Postgraduate School (2018)
38. Zhao, K., Fan, J., Wang, B., Tang, W.: (2020) analytical and experimental study of the vibro-acoustic behavior of a semi-submerged finite cylindrical shell. J. Sound Vib. **482**, 115466 (2020). https://doi.org/10.1016/j.jsv.2020.115466
39. James, J.: Computation of acoustic power, vibration response and acoustic pressures of fluid-filled pipes. NASA STI/Recon Tech. Rep.N **82**, 32630 (1982)

40. Fuller, C.: Radiation of sound from an infinite cylindrical elastic shell excited by an internal monopole source. J. Sound Vib. **109**(2), 259–275 (1986)
41. Abramowitz, M., Stegun, I.A.: Handbook of Mathematical Functions with Formulas, Graphs, and Mathematical Tables, vol. 55. US Government printing office, Washington, D.C. (1968)
42. Maxit, L., Ginoux, J.-M.: Prediction of the vibro-acoustic behavior of a submerged shell non periodically stiffened by internal frames. J. Acoust. Soc. Am. **128**(1), 137–151 (2010). https://doi.org/10.1121/1.3436526